Prediction of Transonic Limit-Cycle Oscillations Using an Aeroelastic Harmonic Balance Method

Yao, W., & Marques, S. (2015). Prediction of Transonic Limit-Cycle Oscillations Using an Aeroelastic Harmonic Balance Method. *AIAA Journal*, *53*(7), 2040-2051. https://doi.org/10.2514/1.J053565

Published in:
AIAA Journal

Document Version:
Peer reviewed version

Queen's University Belfast - Research Portal:
Link to publication record in Queen's University Belfast Research Portal

Prediction of Transonic Limit Cycle Oscillations using an Aeroelastic Harmonic Balance Method

Journal:	*AIAA Journal*
Manuscript ID:	2014-04-J053565.R2
Manuscript Type:	Full Paper
Date Submitted by the Author:	18-Jan-2015
Complete List of Authors:	Yao, Weigang; Queen's University Belfast, Mechanical and Aerospace Marques, Simão; Queen's University Belfast, Mechanical and Aerospace
Subject Index Category:	00200 Aeroelasticity and Aeroservoelasticity < 00000 AIRCRAFT TECHNOLOGY, CONVENTIONAL, STOL/VTOL, 20500 Computational Fluid Dynamics < 20000 FLUID DYNAMICS, 00100 Aerodynamics < 00000 AIRCRAFT TECHNOLOGY, CONVENTIONAL, STOL/VTOL
Select ONE Subject Index for the Table of Contents. This is where your paper will show up in the Table of Contents:	00000 AIRCRAFT TECHNOLOGY, CONVENTIONAL, STOL/VTOL

Prediction of Transonic Limit Cycle Oscillations using an Aeroelastic Harmonic Balance Method

W. Yao[1] and S. Marques[2].
School of Mechanical and Aerospace Engineering,

Queen's University Belfast, Belfast, UK, BT9 5AH

This work proposes a novel approach to compute transonic Limit Cycle Oscillations (LCOs) using high fidelity analysis. CFD based Harmonic Balance (HB) methods have proven to be efficient tools to predict periodic phenomena. This paper's contribution is to present a new methodology to determine the unknown frequency of oscillations, enabling HB methods to accurately capture LCOs ; this is achieved by defining a frequency updating procedure based on a coupled CFD/CSD (Computational Structural Dynamics) HB formulation to find the LCO condition. A pitch/plunge aerofoil and delta wing aerodynamic and respective linear structural models are used to validate the new method against conventional time-domain simulations. Results show consistent agreement between the proposed and time-marching methods for both LCO amplitude and frequency, while producing at least one order of magnitude reduction in computational time.

NOMENCLATURE

$\mathbf{A}$ = Harmonic Balance frequency domain matrix

b, c = aerofoil semi-chord and chord, respectively

CFL = Courant-Friedrichs-Lewy

$\mathbf{D}$ = Harmonic Balance operator matrix

E = energy

$\mathbf{E}$ = Transformation matrix between frequency and time domains

$\mathbf{f}$ = fluid force acting on structure

$\mathbf{F}, \mathbf{G}, \mathbf{H}$ = convective fluxes for fluid equations

h = plunge coordinate

$\mathbf{I}$ = HB residual

$\mathbf{K}$ = structure stiffness matrix

$\mathbf{L}$ = frequency updating figure of merit

$\mathbf{M}$ = structure mass matrix

p = pressure

$\mathbf{R}$ = vector of fluid and/or structural equation residual

t = time step

U_∞ = free-stream velocity

u, v, w = fluid cartesian velocity components

V, V_s = reduced velocity and velocity index

$\mathbf{W}$ = vector of fluid unknowns

$\mathbf{x}, \mathbf{y}$ = vector of structural unknowns

α = angle of attack

ω, κ = frequency and reduced frequency, $\kappa = \frac{2\omega}{U_\infty c}$

ρ = density

τ = pseudo-time step

I. Introduction

Industry standard practices to solve aeroelastic problems rely heavily upon linear aerodynamic theory. This has well known limitations in the transonic regime and where other sources of aerodynamic non-linearities are present (e.g., unsteady viscous flows), hence a clear need for physics based modeling tools has emerged as identified by Noll *et al.*[3]. When nonlinearities are present, aeroelastic instabilities can lead to oscillations that become limited and LCOs are observed. This is a problem of considerable practical interest and is well documented for in-service aircraft [4, 5]. The presence of nonlinearities, either structural or aerodynamic, poses additional challenges both in terms of complexity and computational resources, by requiring higher-fidelity analysis. Such requirements can be exacerbated by the need to quantify the uncertainty due to unknown or variable parameters[6, 7]. Hence, several efforts have been made to address both issues of retaining the required level of fidelity to capture the relevant physics, while at the same time limiting the computational resources required for such analysis.

To overcome these restrictions, CFD methods can be coupled with CSD tools in the time domain; however this type of analysis is used as a last resort tool due to the high computational cost. For several years, the research community has developed Reduced Order Models (ROM) to avoid the penalty of full order time domain analysis. Several methods have been proposed and used, for example: Proper Orthogonal Decomposition (POD)[8, 9], Volterra Series[10–12], Neural Networks[13]. Typically, ROMs lack generality as their application is dependent on the original parameters used in building the ROM.

To avoid such restrictions, model reduction based on centre manifold theory has shown the ability to predict LCOs without compromising the underlying physics of the problem[7, 14]. An alternative to ROM and full time domain analysis of aeroelastic oscillatory problems is to employ the non-linear HB method. New Harmonic Balance methods have been developed for CFD time periodic flows[15, 16]; in such methods, the periodicity of the flow is exploited and represent time dependent flow variables as Fourier series and recast the problem in terms of Fourier coefficients. These methods have been successful in predicting unsteady flows efficiently in diverse applications: forced motions[17, 18], helicopter rotors[19], turbomachinery[15, 20, 21]. Thomas *et al.*extended

the HB formulation to predict LCOs for fixed wing aircraft[5]. Ekici and Hall further reduced the computational cost of predicting LCOs with HB methods, by proposing a *one-shot* method to analyze a one degree-of-freedom (DOF) LCO in turbomachinery flows[20].

As far as the authors are aware, only the method proposed by Thomas *et al.*[5] has been able to predict LCOs for fixed wing aircraft using a CFD based HB formulation. This paper presents an alternative method to compute nonlinear aeroelastic instabilities (LCOs) using a coupled CFD-CSD HB formulation. The main source of nonlinearities of interest in this work are moving shocks, hence the Euler equations for fluid dynamics are solved in conjunction with linear structural models. The paper will first describe the details of the CFD and HB implementations; this will be followed by presenting a novel formulation for predicting LCO amplitudes and frequencies of coupled aeroelastic systems. The method described will be first validated using experimental data from forced motion test cases, then the new Aeroelastic Harmonic Balance (A-HB) method will be used to predict LCOs in 2D and 3D test cases, results are assessed against time marching methods for accuracy and efficiency.

II. Flow Solver

The semi-discrete form of an arbitrary system of conservation laws such as the three-dimensional Euler equations can be described as:

$$\frac{\partial \mathbf{W}}{\partial t} = -\mathbf{R}(\mathbf{W}) \tag{1}$$

where $\mathbf{R}$ is the residual error of the steady-state solution:

$$\mathbf{R} = \frac{\partial \mathbf{F}}{\partial x} + \frac{\partial \mathbf{G}}{\partial y} + \frac{\partial \mathbf{H}}{\partial z} \tag{2}$$

Here $\mathbf{W}$ is the vector containing the flow variables and $\mathbf{F}$, $\mathbf{G}$, $\mathbf{H}$ are the fluxes, which are given by:

$$\mathbf{W} = \begin{bmatrix} \rho \\ \rho u \\ \rho v \\ \rho w \\ \rho E \end{bmatrix}, \quad \mathbf{F} = \begin{bmatrix} \rho u \\ \rho uu + p \\ \rho uv \\ \rho uw \\ u(\rho E + p) \end{bmatrix}, \quad \mathbf{G} \begin{bmatrix} \rho v \\ \rho uv \\ \rho vv + p \\ \rho vw \\ v(\rho E + p) \end{bmatrix}, \quad \mathbf{H} = \begin{bmatrix} \rho w \\ \rho uw \\ \rho vw \\ \rho ww + p \\ w(\rho E + p) \end{bmatrix}, \tag{3}$$

The steady state solution of the Euler equations is obtained by marching the solution forward in time by solving the following discrete nonlinear system of equations:

$$\frac{\mathbf{W}^{n+1} - \mathbf{W}^n}{\Delta t} = -\mathbf{R}^n \tag{4}$$

To discretize the residual convective terms a Roe flux function[22] together with MUSCL interpolation is used[23], the Van Albada limiter is used to obtain 2^{nd} order accuracy. The nonlinear system of algebraic equations represented by eq.(4) is solved by an explicit, 4-stage, Runge-Kutta method.

III. Harmonic Balance Formulation

As discussed in the introduction, several authors have demonstrated the suitability of HB methods as an alternative to time marching CFD formulations for periodic flow problems. To obtain the HB version of the flow solver, we follow the methodology presented by Thomas *et al.*[24], which is summarised next. Consider the semi-discrete form as a system of ordinary differential equations

$$\mathbf{I}(t) = \frac{d\mathbf{W}(t)}{dt} + \mathbf{R}(t) = 0 \tag{5}$$

The solution of $\mathbf{W}$ and $\mathbf{R}$ in eq.(5) can be approximated to be a truncated Fourier series of N_H harmonics with a fundamental frequency ω:

$$\mathbf{W}(t) \approx \hat{\mathbf{W}}_0 + \sum_{n=1}^{N_H} (\hat{\mathbf{W}}_{2n-1} \cos(n\omega t) + \hat{\mathbf{W}}_{2n} \sin(n\omega t)) \tag{6}$$

$$\mathbf{R}(t) \approx \hat{\mathbf{R}}_0 + \sum_{n=1}^{N_H} (\hat{\mathbf{R}}_{2n-1} \cos(n\omega t) + \hat{\mathbf{R}}_{2n} \sin(n\omega t)) \tag{7}$$

Hence, eq.(5) can also be approximated by a truncated Fourier series,

$$\mathbf{I}(t) \approx \hat{\mathbf{I}}_0 + \sum_{n=1}^{N_H} (\hat{\mathbf{I}}_{2n-1} \cos(n\omega t) + \hat{\mathbf{I}}_{2n} \sin(n\omega t)) \tag{8}$$

which results in the following system of equations

$$\hat{\mathbf{I}}_0 = \hat{\mathbf{R}}_0 \tag{9}$$

$$\hat{\mathbf{I}}_{2n-1} = \omega n \hat{\mathbf{W}}_{2n} + \hat{\mathbf{R}}_{2n-1} \tag{10}$$

$$\hat{\mathbf{I}}_{2n} = -\omega n \hat{\mathbf{W}}_{2n-1} + \hat{\mathbf{R}}_{2n} \tag{11}$$

which results in a system of $(2N_H + 1)$ equations for the Fourier coefficients that can be expressed in matrix form as

$$\omega \mathbf{A}\hat{\mathbf{W}} + \hat{\mathbf{R}} = 0 \tag{12}$$

where $\mathbf{A}$ is given by:

$$\mathbf{A} = \begin{bmatrix} 0 & & & \\ & \mathbf{J}_1 & & \\ & & \ddots & \\ & & & \mathbf{J}_{N_H} \end{bmatrix}_{(2N_H+1)\times(2N_H+1)}, \quad \mathbf{J}_n = n \begin{bmatrix} 0 & 1 \\ -1 & 0 \end{bmatrix}, \quad n = 1, 2, \ldots, N_H \tag{13}$$

To overcome the difficulties in expressing the Fourier coefficient in $\hat{\mathbf{R}}$ as functions of $\hat{\mathbf{W}}$, Hall *et al.*[15] proposed to cast the system of equations back in the time domain, where the flow variables and residual solutions are split into $(2N_H + 1)$, discrete, equally spaced intervals over the period $T = \frac{2\pi}{\omega}$.

$$\mathbf{W}_{hb} = \begin{bmatrix} \mathbf{W}(t_0 + \Delta t) \\ \mathbf{W}(t_0 + 2\Delta t) \\ \vdots \\ \mathbf{W}(t_0 + T) \end{bmatrix}, \quad \mathbf{R}_{hb} = \begin{bmatrix} \mathbf{R}(t_0 + \Delta t) \\ \mathbf{R}(t_0 + 2\Delta t) \\ \vdots \\ \mathbf{R}(t_0 + T) \end{bmatrix}, \tag{14}$$

It is possible to define a transformation matrix, $\mathbf{E}$ that relates the frequency domain variables to their HB time domain counterpart[15]

$$\hat{\mathbf{W}} = \mathbf{E}\mathbf{W}_{hb} \quad \hat{\mathbf{R}} = \mathbf{E}\mathbf{R}_{hb} \tag{15}$$

Substituting the terms in eq.(15) in eq.(12), it becomes:

$$\omega \mathbf{A}\hat{\mathbf{W}} + \hat{\mathbf{R}} = 0 = \omega \mathbf{A}\mathbf{E}\mathbf{W}_{hb} + \mathbf{E}\mathbf{R}_{hb} = \omega \mathbf{E}^{-1}\mathbf{A}\mathbf{E}\mathbf{W}_{hb} + \mathbf{R}_{hb} =$$

$$= \omega \mathbf{D}\mathbf{W}_{hb} + \mathbf{R}_{hb} = 0 \tag{16}$$

where $\mathbf{D} = \mathbf{E}^{-1}\mathbf{A}\mathbf{E}$, the elements in matrix $\mathbf{D}$ are given by:

$$\mathbf{D}_{i,j} = \frac{2}{2N_H + 1} \sum_{k=1}^{N_H} k \sin\left(\frac{2\pi k(j-i)}{2N_H + 1}\right) \tag{17}$$

To solve eq.(16) a pseudo time step of the form is introduced:

$$\frac{d\mathbf{W}_{hb}}{d\tau} + \omega \mathbf{D}\mathbf{W}_{hb} + \mathbf{R}_{hb} = 0 \tag{18}$$

To solve eq.(18), any steady-state CFD time marching method can be used. In this work an explicit 4-stage Runge-Kutta scheme is employed. The solution to eq.(18) corresponds to the flow solution at $2N_H + 1$ equally spaced time sub levels. The Fourier coefficients can be obtained by applying the transformation matrix $\mathbf{E}$, and the flow field at any time level can be recovered by using Fourier expansions on the flow variables.

IV. Aeroelastic Formulation

Consider a generic dynamic system without damping, whose behaviour can be described using the equations of motion given by:

$$\mathbf{M}\ddot{\mathbf{x}} + \mathbf{K}\mathbf{x} = \mathbf{f} \tag{19}$$

where $\mathbf{M}$, $\mathbf{K}$, respectively, represent the mass and stiffness of the system and $\mathbf{f}$ is an external force (in this work, this will be the aerodynamic force, $\mathbf{f} = \mathbf{f}(\mathbf{w}, \omega, \mathbf{x})$). This equation can be transformed into a state-space form, giving:

$$\dot{\mathbf{y}} = \mathbf{A_s}\mathbf{y} + \mathbf{B_s}\mathbf{f} \tag{20}$$

where:

$$\mathbf{A_s} = \begin{bmatrix} 0 & \mathbf{I} \\ -\mathbf{M}^{-1}\mathbf{K} & 0 \end{bmatrix}, \quad \mathbf{B_s} = \begin{bmatrix} 0 \\ \mathbf{M}^{-1} \end{bmatrix}, \quad \mathbf{y} = \begin{bmatrix} \mathbf{x} \\ \dot{\mathbf{x}} \end{bmatrix} \tag{21}$$

Equation (20) has a similar form to the flow equations, hence it can be solved using the HB method described in the previous section, resulting in the following HB format of eq.(20):

$$\omega \mathbf{D}\mathbf{y}_{hb} = \mathbf{A}_s\mathbf{y}_{hb} + \mathbf{B}_s\mathbf{f}_{hb} \tag{22}$$

where $\mathbf{D}$ is the same HB operator described in eq.(17). Equation (22) can be solved using the same pseudo time technique previously presented, leading to the following system of equations[20]:

$$\frac{d\mathbf{y}_{hb}}{d\tau} + \omega \mathbf{D}\mathbf{y}_{hb} - (\mathbf{A}_s\mathbf{y}_{hb} + \mathbf{B}_s\mathbf{f}_{hb}) = 0 \tag{23}$$

Equation (18) together with eq.(23) represent the nonlinear coupled aeroelastic system; when solving the aeroelastic system of equations, at each iteration, the generalized aerodynamic forces are computed using eq.(18), which will feed into eq.(23). The solution from eq.(23) will provide new generalized displacements and velocities for eq.(18). The CFD grid is deformed using Transfinite Interpolation and the mesh velocities are approximated by finite-differences[13].

A. Prediction of Limit-Cycle Oscillations

The prediction of LCO depends on determining a solution vector for $[\omega, \mathbf{y}]$ (the subscript *hb* is dropped for simplicity), that satisfies both the structural governing equation eq.(23) and eq.(18). If the LCO frequency, ω, is given beforehand, then the coupling itself becomes a fixed point iteration process which is extensively used for static aeroelastic problems in its time domain counterpart[18]. A straightforward method to search for solutions for LCO is to employ a Newton-Raphson method[25]. From eq.(22) define the following residual:

$$\mathbf{R}(\omega, \mathbf{y}) = \omega \mathbf{D}\mathbf{y} - (\mathbf{A}_s \mathbf{y} + \mathbf{B}_s \mathbf{f}) \tag{24}$$

Applying the Newton-Raphson method to eq.(24), we get:

$$\begin{bmatrix} \omega \\ \mathbf{y} \end{bmatrix}_{n+1} = \begin{bmatrix} \omega \\ \mathbf{y} \end{bmatrix}_{n} - \lambda \mathbf{J}^{-1} \mathbf{R}(\omega_n, \mathbf{y}_n) \tag{25}$$

Where $\mathbf{J}$ is the Jacobian of $\mathbf{R}$ with respect to the solution vector $[\omega, \mathbf{y}]$ and λ is a relaxation parameter, usually equal to one; the expensive part is to approximate the derivatives of $\mathbf{f}$ with respect to $[\omega, \mathbf{y}]$ by finite differencing. If the number of harmonics used in eq.(18) is N_H, the structural degrees-of-freedom is N_s, then the fluid system needs to be evaluated $(N_s[(2N_H + 1) \times 2] + 1)$ times to form $\mathbf{J}$. As long as the initial guess is *good enough*, the Newton-Raphson method usually achieves converged solutions rapidly and efficiently. Thomas *et al.*[25] demonstrated the effectiveness of this method for LCO prediction. For higher number of harmonics and structural DOF, the computational cost of building the Jacobian $\mathbf{J}$ itself is significant[17], and thus makes the Newton-Raphson method less attractive. Ekici and Hall[20] developed a *one-shot* determination approach by advancing the structural and fluid system to convergence at the same time, with frequency updating. The authors demonstrate that the overall computational cost is lower than the Newton-Raphson method for a

2D turbomachinery problem, with a single DOF structural governing equation. As shown before, a pseudo time marching strategy can be adopted to solve eq.(23) [20]:

$$\frac{\partial \mathbf{y}}{\partial \tau} + \omega \mathbf{D}\mathbf{y} - (\mathbf{A}_s\mathbf{y} + \mathbf{B}_s\mathbf{f}) = 0$$

The convergence of eq.(23) is highly dependent on the time step size, τ; in other words, τ should be large enough to march eq.(23) rapidly to convergence and at the same time ensure numerical stability. However, unlike the fluid system where local time step size can be used, for the HB system in eq.(23), a constant value is required. However, as the structural DOF increases, a significant deterioration of the convergence rate for eq.(23) was observed, even when using an implicit algorithm formulation.

To determine the LCO condition using eq.23, the frequency updating can be achieved by minimizing the L_2 norm of the residual $\mathbf{R}$ of eq.(24)[20]. First, define a figure of merit, in this case:

$$\mathbf{L}_n = \frac{1}{2}\mathbf{R}^T\mathbf{R} = \frac{1}{2}\left[\omega\mathbf{D}\mathbf{y} - (\mathbf{A}_s\mathbf{y} + \mathbf{B}_s\mathbf{f})\right]^T\left[\omega\mathbf{D}\mathbf{y} - (\mathbf{A}_s\mathbf{y} + \mathbf{B}_s\mathbf{f})\right] \tag{26}$$

Then derive the first order derivative with respect to ω:

$$\frac{\partial \mathbf{L}_n}{\partial \omega} = (\mathbf{D}\mathbf{y})^T\left[\omega\mathbf{D}\mathbf{y} - (\mathbf{A}_s\mathbf{y} + \mathbf{B}_s\mathbf{f})\right] \tag{27}$$

For a given vector $[\mathbf{y}, \mathbf{f}]$, the frequency can be solved directly by manipulating small matrices. It is worth noting that eq.(27) is derived with the force vector $\mathbf{f}$ frozen. The results presented below demonstrate that this assumption makes updating the frequency difficult and slow for multiple DOF systems.

B. Proposed Approach for LCO Predictions

Inspired by the results of Blanc *et al.*[18], the present work aims to transform this LCO prediction problem into a fixed point algorithm with frequency updating. As before, the basic idea is to solve the linear eq.(22) for a given combination of $[\omega, \mathbf{f}]$, then transfer the displacement back to the fluid system. As in eq.(26), the frequency is updated by minimizing the residual $\mathbf{R}$ but, critically, without freezing the aerodynamic forces $\mathbf{f}$, leading to:

$$\frac{\partial \mathbf{L}_n}{\partial \omega} = \left(\mathbf{D}\mathbf{y} - \mathbf{B}_s\frac{\partial \mathbf{f}}{\partial \omega}\right)^T\left[\omega\mathbf{D}\mathbf{y} - (\mathbf{A}_s\mathbf{y} + \mathbf{B}_s\mathbf{f})\right] \tag{28}$$

If the frequency ω is not at the LCO condition, the residual $\mathbf{R}$ for the displacement is not able to converge. Therefore, the idea is to update the frequency at every n_i iterations.

The new algorithm is represented in Algorithm 1. When compared to the standard fixed point algorithm described by Blanc *et al.*[18], the new algorithm introduces some extra computational effort to compute the gradient of the aerodynamic force with respect to the frequency. However, the frequency is only updated every n_i iterations (numerical experiments show that 10-15 iterations are an adequate compromise between robustness and efficiency) and the perturbation is sufficiently small, minimizing the computational cost. The additional computational cost of updating the frequency is largely dependent on the approximation of the aerodynamic force gradient, adding about 50% of the cost of solving eq.(18).

Algorithm 1: Aeroelastic Harmonic Balance

begin
  $[\omega_0, \mathbf{y}_0, \mathbf{f}_0] \longleftarrow$ Initialize variables
  while $[\omega, \mathbf{y}, \mathbf{f}]$ *not converged* **do**
    $n \longleftarrow n + 1$
    $\mathbf{y} \longleftarrow \mathbf{R}(\omega, \mathbf{y}, \mathbf{f})$ ▷ `Linear Solve of eq.`(22)
    $\mathbf{y} \longleftarrow \lambda \mathbf{y}$ ▷ `relax y`
    $\mathbf{f} \longleftarrow$ HB-CFD solver ▷ `march forward CFD solution, eq.`(18)
    if $MOD(n, n_i) == 0$ **then**
      $\omega \longleftarrow \omega_n$ ▷ `update` ω
      $\omega \longleftarrow \lambda\omega$ ▷ `relax` ω
    end
  end
end

V. Results

A. Code Validation

The AGARD CT5[26] case is chosen to validate the HB-CFD code. This case is a prescribed pitching NACA 0012 aerofoil, the flow condition and motion parameters are detailed in Table 1.

Case	M_∞	α_m	α_0	k	x_m
CT5	0.755	0.016°	2.51°	0.0814	0.25

Table 1 CT5 Case Parameters

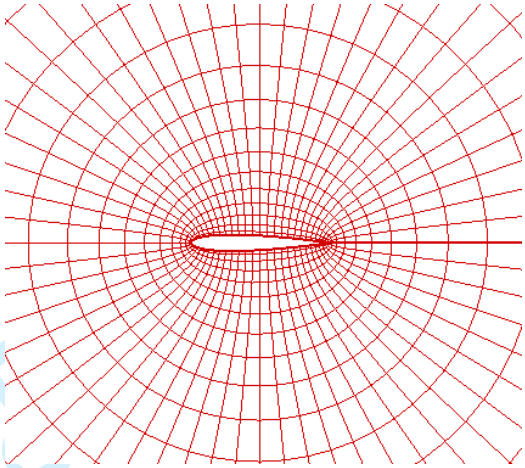

Fig. 1 O-grid over NACA 0012 aerofoil

An O-type grid as the one shown in Fig. 1 was used. A grid convergence study is carried out in terms of lift and moment coefficients. Five harmonics are used for all the results shown in Fig. 2. It is clearly shown in Fig. 2 that a 61×21 grid captures the details of the unsteady lift and moment coefficients adequately. The experimental data is also included for comparison. All numerical methods produce identical results; with respect to the experiment, the lift coefficient is consistently under predicted and small discrepancies are observed for the moment coefficient at about 1° incidence. These discrepancies are consistent with the results reported in the literature[27–29]. Additionally, a convergence study concerning the number of harmonics required to accurately recreate the periodic forces is also carried out and the results are shown in Fig. 3, which demonstrate that three harmonics are sufficient to obtain converged lift and pitching moment coefficient predictions predictions. A subsequent convergence study with respect to LCO amplitude and frequency is also performed.

B. LCO Predictions

In order to validate the coupling approach proposed in this paper, a pitch/plunge symmetric NACA 64A010 aerofoil, shown in Fig. 4, is used to assess its efficiency and effectiveness. The

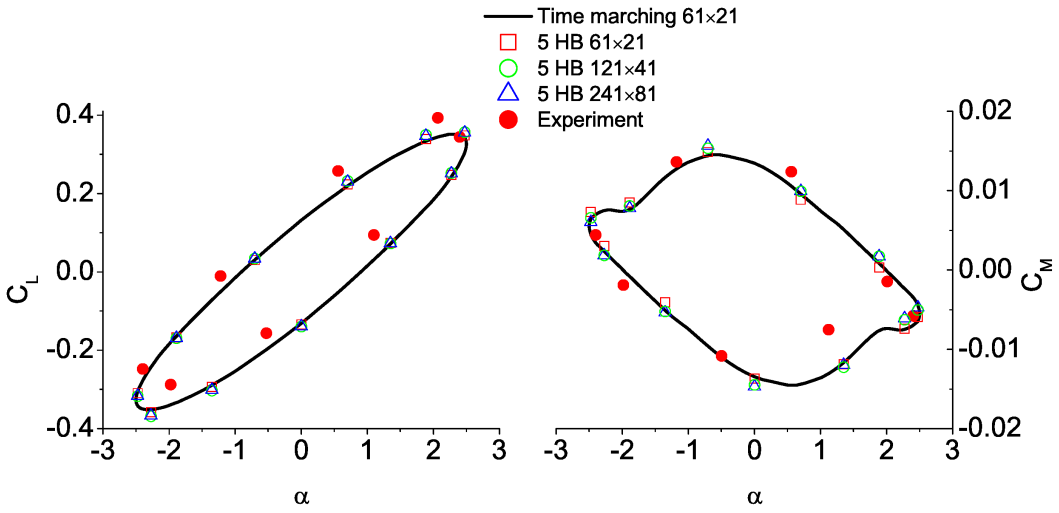

Fig. 2 Grid Convergence Study for CT5 Case

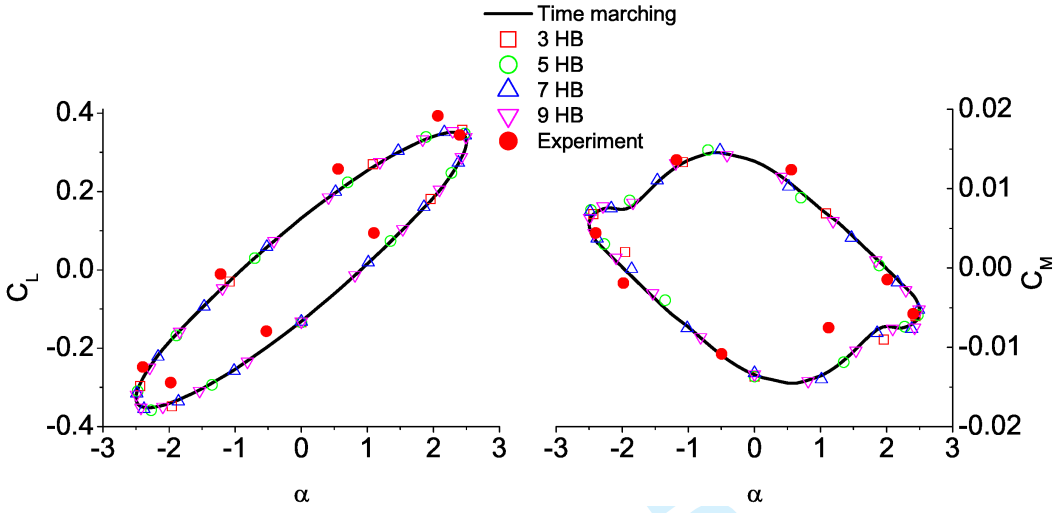

Fig. 3 Number of Harmonics Convergence Study for CT5 Case - 61×21 grid

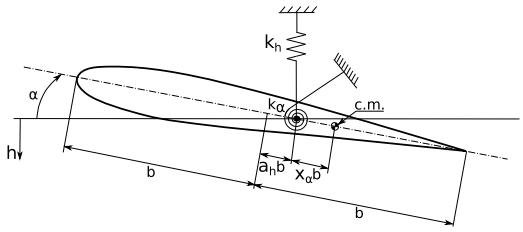

Fig. 4 Diagrammatic representation of pitch/plunge, two-degree-of-freedom aerofoil

Static unbalance, $x_\alpha = S_\alpha/mb$	0.25
Radius of gyration about elastic axis, $r_\alpha^2 = I_\alpha/mb^2$	0.75
Frequency ratio, ω_h/ω_α	0.5
Mass ratio, $\mu = m/\pi\rho_\infty b^2$	75

Table 2 Pitch/Plunge Aerofoil Parameters

equations of motion for this pitch-plunge aerofoil problem can be found in reference:[25]

$$m\ddot{h} + S_\alpha\ddot{\alpha} + K_h = -q_\infty c C_l \tag{29}$$

$$S_\alpha\ddot{h} + I_\alpha\ddot{\alpha} + K_\alpha = q_\infty c^2 C_m \tag{30}$$

where m is the mass of the aerofoil, S_α, I_α are the first and second moment of inertia about the elastic axis, respectively; q_∞ represents the dynamic pressure and C_l, C_m are the lift and pitching moment coefficient.

Following Thomas *et al.*[25], the non-dimensional form of eq.(29) and (30) is given by

$$\mathbf{M}\ddot{\mathbf{y}} + \frac{1}{V^2}\mathbf{K}\mathbf{y} = \frac{4}{\pi\mu}\mathbf{f} \tag{31}$$

where

$$\mathbf{M} = \begin{bmatrix} 1 & x_\alpha \\ x_\alpha & r_\alpha^2 \end{bmatrix}, \quad \mathbf{K} = \begin{bmatrix} \left(\frac{\omega_h}{\omega_\alpha}\right)^2 & 0 \\ 0 & r_\alpha^2 \end{bmatrix}, \quad \mathbf{f} = \begin{bmatrix} -C_l \\ 2C_m \end{bmatrix}, \quad \mathbf{y} = \begin{bmatrix} \frac{h}{b} \\ \alpha \end{bmatrix}, \quad V = \frac{U_\infty}{\omega_\alpha c} \tag{32}$$

and the structural parameters are given in Table 2.

Besides the above parameters, the Mach number and the initial angle of attack are set to 0.8 and 0°, respectively, the aeroelastic axis distance from the centre chord is: $a_h/b = -0.6$. The velocity index is used to set different conditions (e.g.: dynamic pressure, altitude) for the analysis. For a given value of the velocity index, eq.(31) is solved using the procedure described in the section IV B, determining the final amplitude and frequency of the periodic motion. The velocity index is defined as:

$$V_s = \frac{U_\infty}{b\omega_\alpha\sqrt{\mu}} \tag{33}$$

Following the proposed algorithm 1, the Aeroelastic-HB solver needs to initialize the structural and fluid systems $[\omega, \mathbf{y}, \mathbf{f}]$. The critical part is how to determine the initial frequency. Once the

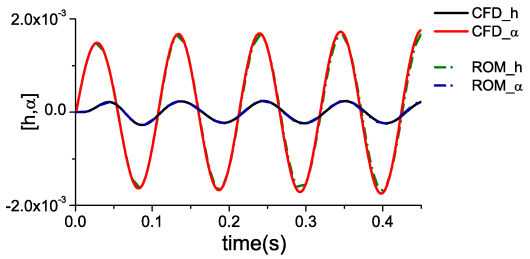

Fig. 5 Pitch/plunge aerofoil flutter response

frequency is determined the coupling algorithm becomes a fixed point problem, leading to a very fast convergence of the coupled problem, as illustrated by Blanc *et al.*[18], even over relative large margins of the initial values of the displacement $\mathbf{y}$. The LCOs investigated in this work, occur in a post-flutter regime, hence the initial frequency used for the LCO prediction will be close to the flutter condition. Volterra series along with the ERA (*Eigensystem Realization Algorithm*) method, as described in references [10, 30] is employed to construct a 20-DOF linear CFD-ROM coupled with the 2-DOF structural model to determine the onset of flutter. The full-order CFD and ROM prediction for this aerofoil case is shown in Fig. 5; full details of this method can be found in reference[30]. The flutter condition using the reduced frequency is $[\kappa, V_s] = [0.1089, 0.693]$.

Beyond the flutter point V_s, it is expected for the oscillations to become bounded and form a finite amplitude oscillation or LCO, due to the nonlinear aerodynamic force. Without loss of generality, the starting point is chosen to be $[\kappa, V_s] = [0.1, 0.725]$, meaning an LCO at $V_s = 0.725$ needs to be computed with an initial reduced frequency guess $\kappa = 0.1$ which is very close to the flutter condition. As described in the coupling algorithm, the fluid system is initialized with $[\kappa, V_s] = [0.1, 0.725]$ and an initial displacement given by: $\mathbf{y} = [0.2, 0.02rad]^T$. Figure 6 shows the fluid system convergence history during the A-HB calculations. The residual drops monotonically, note that once the residual is below the level of 10^{-5}, the fluid force is no longer varying significantly.

The main purpose of this test case is to evaluate the solver, particularly the frequency updating procedure. Figure 7-a) shows the frequency converging rapidly in fewer than 500 iterations for $V_s = 0.725$ to a value of $\kappa = 0.1055$, approximately 5% above the initial value. Once the LCO is

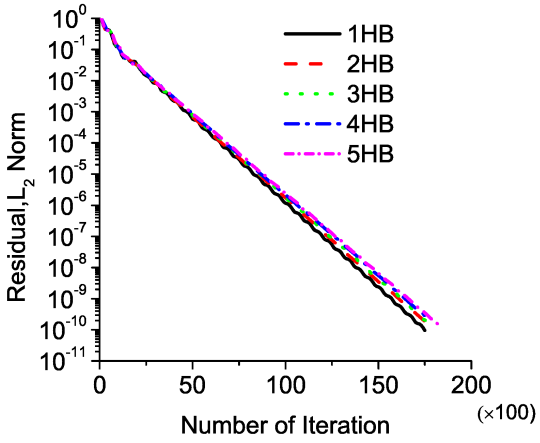

Fig. 6 Cumulative Runge-Kutta Iterations required to converge HB-CFD system

N. Harmonics	ω/ω_{LCO} $(V_s = 0.725)$	ω/ω_{LCO} $(V_s = 0.80)$
1 Harmonics	0.995738669	0.986594291
2 Harmonics	0.999688033	0.999869965
3 Harmonics	0.999636829	0.999097819
4 Harmonics	0.999963967	0.999147212
5 Harmonics	1.000048360	1.000074594

Table 3 Ratios between frequencies predicted by the A-HB and time-marching methods

captured, then the intuitive way to compute LCO at different conditions is to use $[\omega, \mathbf{y}, \mathbf{f}]_{V_s=0.725}$ as the initial guess. Therefore the frequency computed at $V_s = 0.725$ is used for LCOs predictions at $V_s = 0.8$; the initial perturbation remains the same, $\mathbf{y} = [0.2, 0.02rad]^T$. Results are illustrated in Fig. 7-b), it takes fewer than 400 iterations for the frequency to converge at the new velocity index. Both these results converge to LCO frequency values computed using conventional time marching methods, noted in the graphs as the fixed ω_LCO. The impact of using additional harmonics is given by Table 3; the values obtained with one-harmonic are, for most cases, within 1% of the time-marching frequency prediction and retaining more harmonics gives virtually identical results to the conventional approach.

The performance of the updating procedures using either eq.(27) or eq.(28) are assessed in Fig. 7-c) and 7-d). The results suggest that by including the aerodynamic force gradient with respect

to ω, the overall computational cost is decreased; both LCO frequency and amplitude converge significantly faster using the new procedure proposed in this paper. Figure 8 shows the displacement convergence when using a fixed value for ω and when solving for ω using eq.(28). The displacement converges faster when ω is fixed, as expected. It also indicates once the frequency converges, the displacement should converge very rapidly.

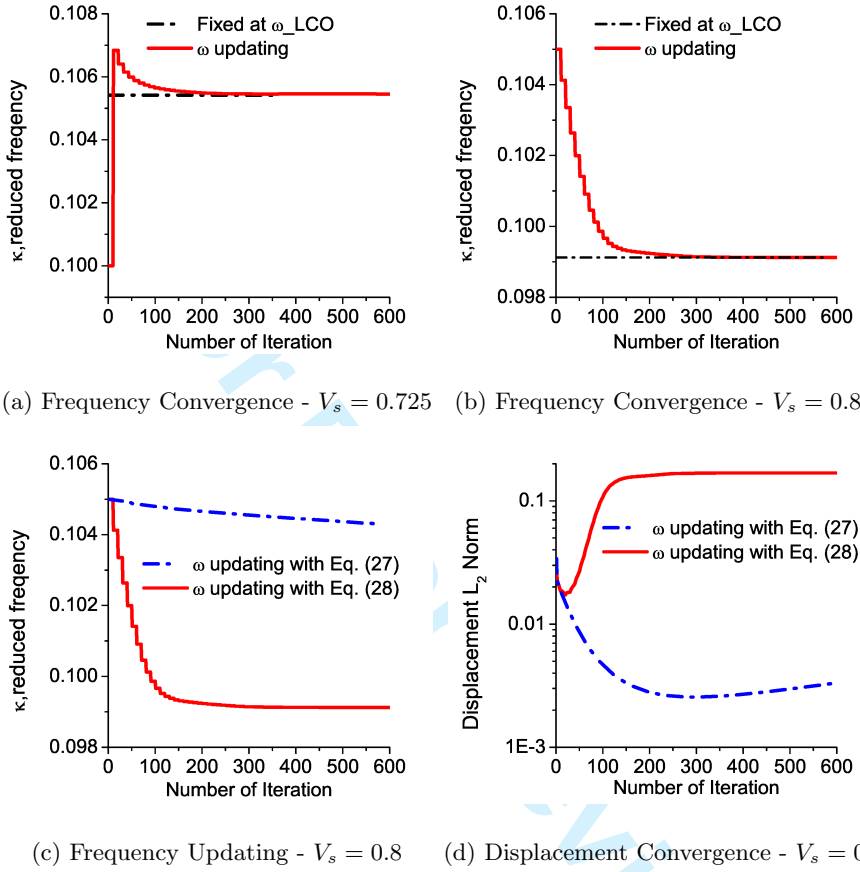

(a) Frequency Convergence - $V_s = 0.725$ (b) Frequency Convergence - $V_s = 0.80$

(c) Frequency Updating - $V_s = 0.8$ (d) Displacement Convergence - $V_s = 0.8$

Fig. 7 A-HB Frequency and amplitude LCO convergence

This test case is also used to assess the impact of retaining different number of harmonics on the LCO amplitudes. Figure 9 shows the position-velocity diagram for both plunge and pitch variables, retaining up to five harmonics. The LCO cycle shown by the continuous line, is reconstructed by the A-HB solution using 90 points. The difference between retaining two, three, four or five harmonics is negligible. A detailed example of the reconstruction cycle by the A-HB for $V_s = 0.8$ is given in Fig. 10, in this case retaining two harmonics slightly under-predicts the motion's amplitudes, hence subsequent calculations are performed retaining three harmonics.

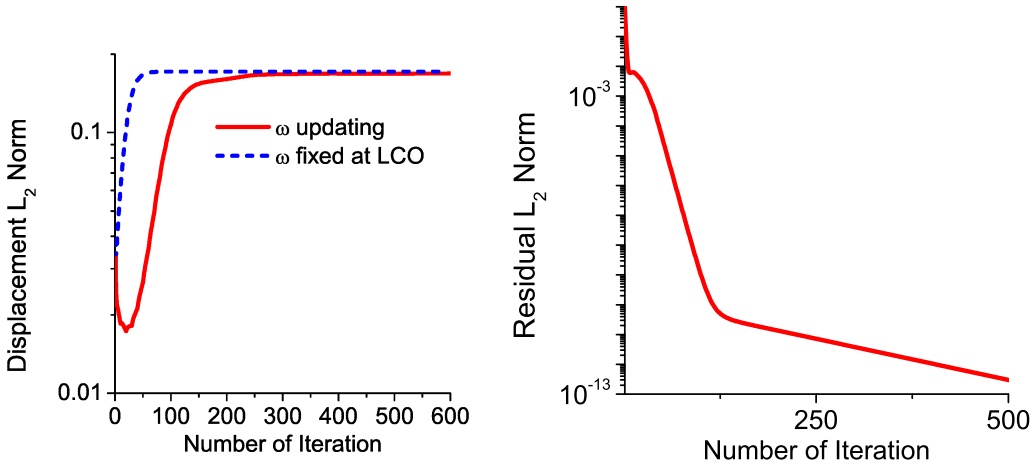

(a) - Displacement (b) Structural Residual

Fig. 8 Convergence of aeroelastic system, fixed ω - $V_s = 0.80$

Δt	h_{max}	α_{max}
1.0×10^{-3}	0.30815	0.04082
5.0×10^{-4}	0.30549	0.04054
2.5×10^{-4}	0.30437	0.04043
1.25×10^{-4}	0.30391	0.04038

Table 4 Time step size convergence at $V_s = 0.80$

A comparison between the LCO solutions, using position-velocity diagrams, obtained by the A-HB method (using three harmonics) and time marching results using a time step of 2.5×10^{-4}, is given in Fig. 11 and 12, showing a good level of agreement. The use of larger time steps still allows for the capture of the LCO, however, it also led to over-predicting the amplitude of the motion, hence not providing a reliable benchmark to the A-HB method. Table 4 provides the time-step size convergence study used in this work.

A comparison of the transonic pressure field at the maximum and minimum positions during the cycle are given in Fig. 13. The shock-wave motion captured by the A-HB method is clearly visible and closely matches the time-marching predictions, there are small differences with respect to time-marching results when using three harmonics, which vanish when five harmonics are retained. The LCO amplitude growth predicted by the A-HB method, retaining three harmonics, is compared against a time marching method in Fig. 14, showing consistent results for all conditions analysed.

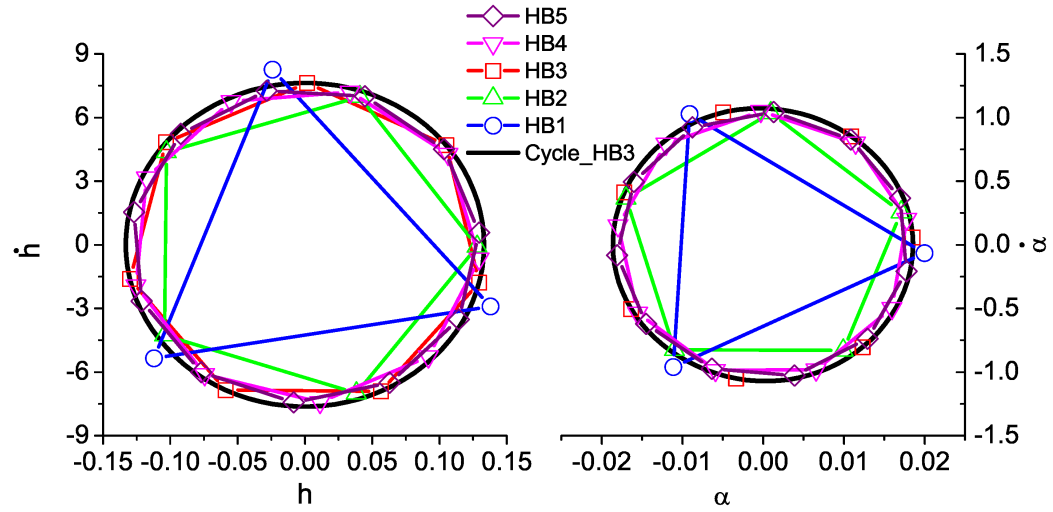

Fig. 9 Position - Velocity diagram at LCO condition - $V_s = 0.725$ - Harmonic Convergence

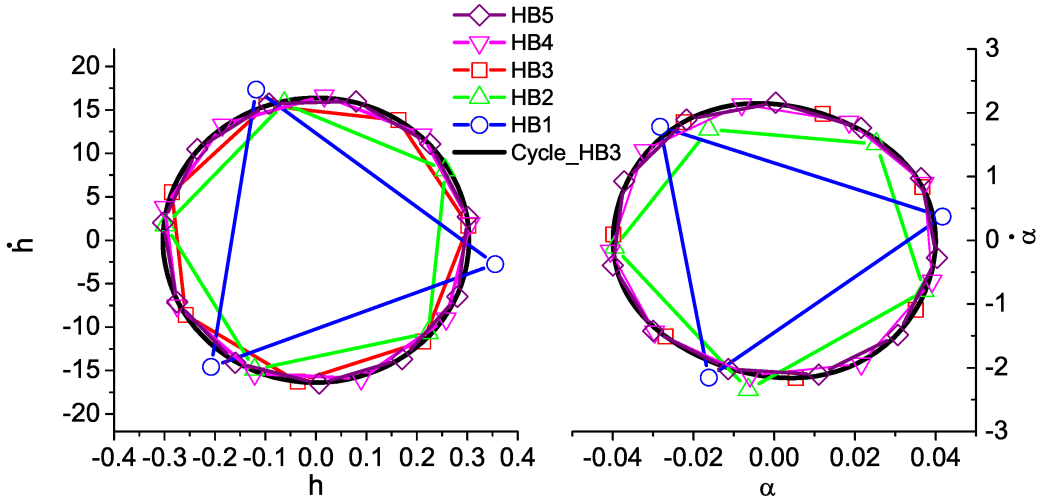

Fig. 10 Position - Velocity diagram at LCO condition - $V_s = 0.80$ - Harmonic Convergence

The effects of increasing the velocity index is shown in detail in Fig. 14-a)-b); increasing the velocity index produces a supercritical LCO. The impact of increasing the frequency ratio of the normal modes, shown in Fig. 14-c)-d), also produces a supercritical LCO, however the initial sensitivity of the amplitude to this parameter is higher. In both parametric changes and for higher amplitudes, the A-HB shows excellent agreement with time-marching results. Furthermore, the results for the conditions tested here are consistent with the equivalent case reported in Thomas *et al.*[25]. Note that the flutter point is under-predicted by the Volterra/ERA ROM, this is due to a larger time step

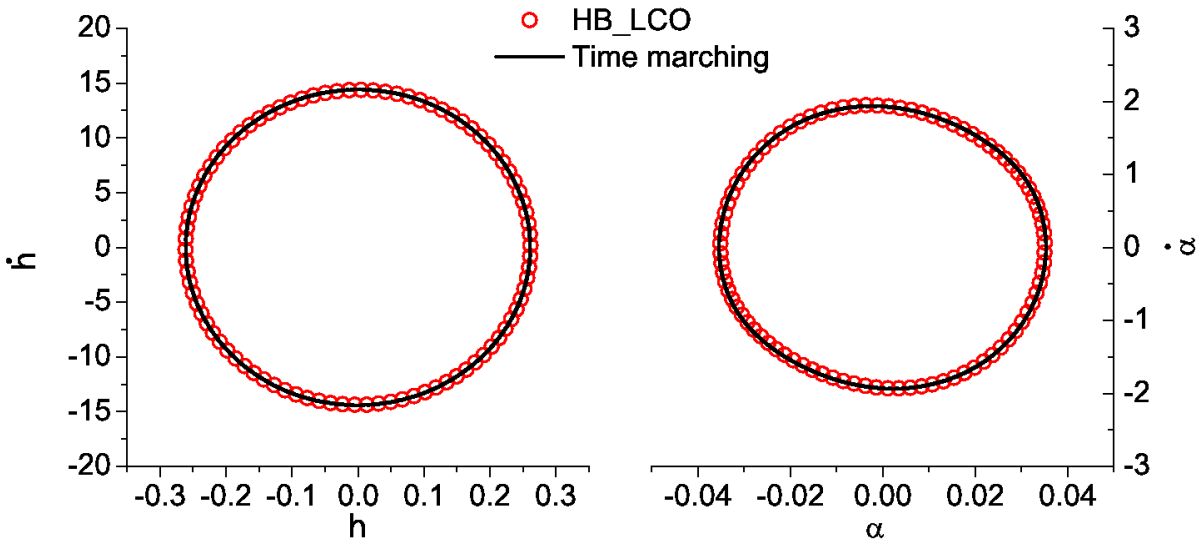

Fig. 11 Comparison between A-HB and time marching LCO solutions - $V_s = 0.775$

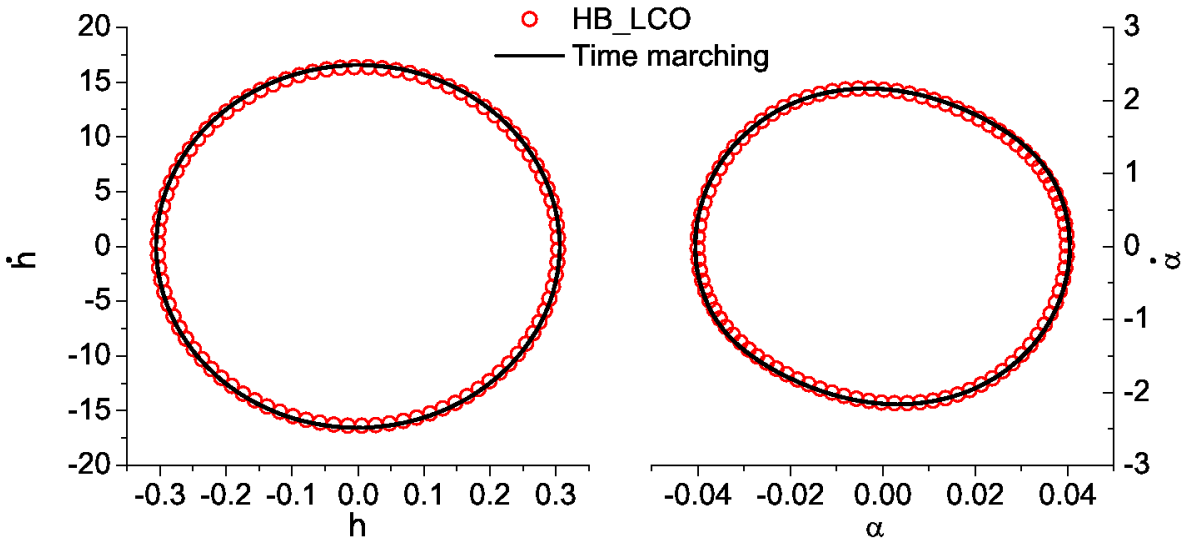

Fig. 12 Comparison between A-HB and time marching LCO solutions - $V_s = 0.80$

($\Delta t = 1.0 \times 10^{-3}$) used when building the ROM, this has little or no impact on the performance of the A-HB method as the flutter prediction is only used to provide the initial frequency input.

The increase in the number of harmonics retained to solve the unsteady problem can have a significant impact on the computational effort required. Figure 15 shows the ratio of the wall clock time required for the time marching calculations to converge with respect to the convergence time when using different number of harmonics. Results include comparisons with two different time-step

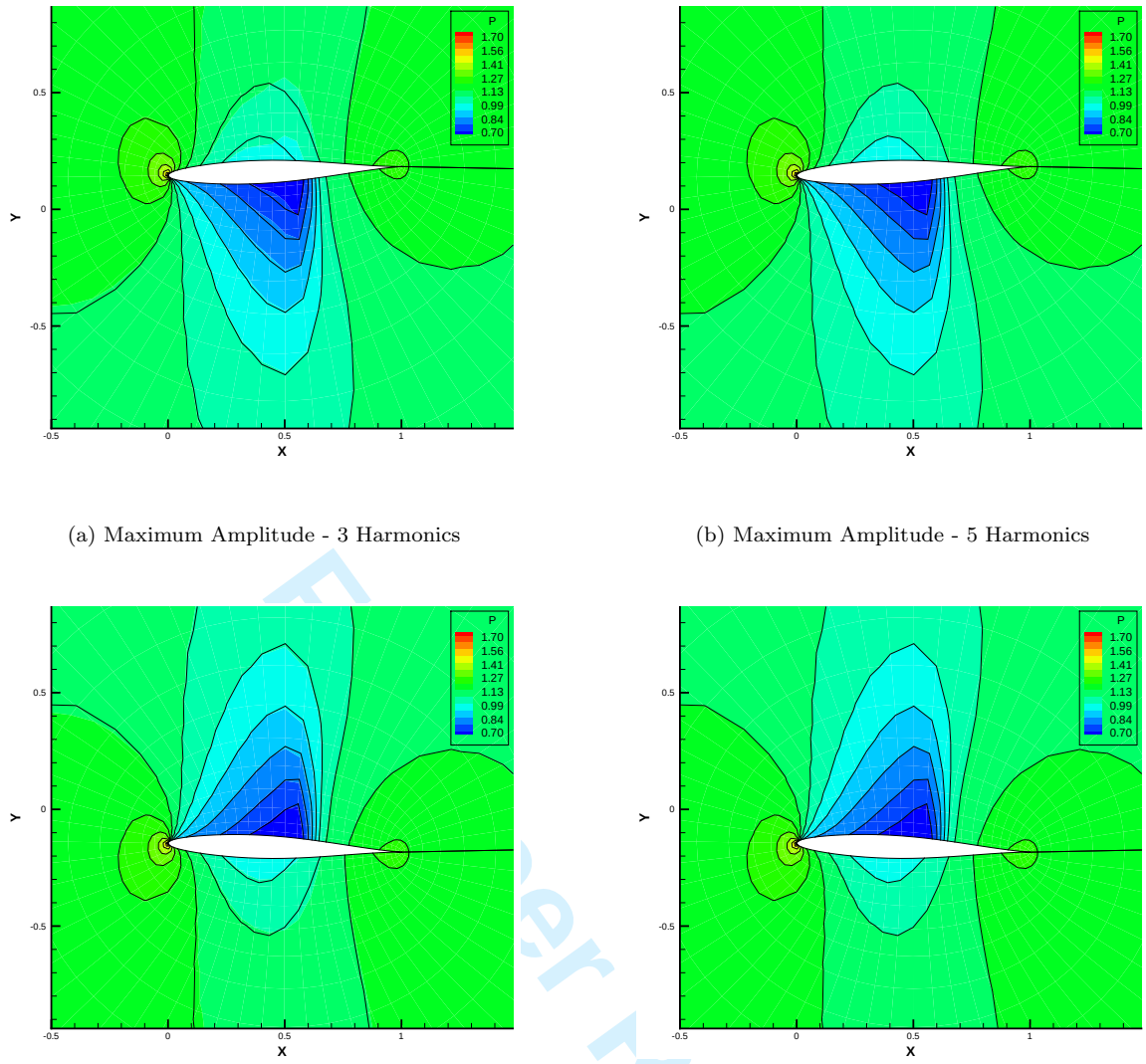

(a) Maximum Amplitude - 3 Harmonics

(b) Maximum Amplitude - 5 Harmonics

(c) Minimum Amplitude - 3 Harmonics

(d) Minimum Amplitude - 5 Harmonics

Fig. 13 Pressure field at extremes of each period at $V_s = 0.8$, contours represent A-HB solutions, solid lines represent time-marching solutions.

sizes used in the time-marching calculations, both curves show a large drop in performance when increasing the number of harmonics retained from one to three. Increasing the number of harmonic modes from three to five incurs a smaller penalty. Results indicate that up to this point, increasing the number of harmonics has a smaller impact on the frequency and structural residual convergence algorithm than, for example, on the cost of solving the CFD system alone. For calculations requiring seven or more harmonics, the CFL number for the CFD calculation has to be reduced significantly, resulting in long computational times, i.e. similar to those required by time-marching methods.

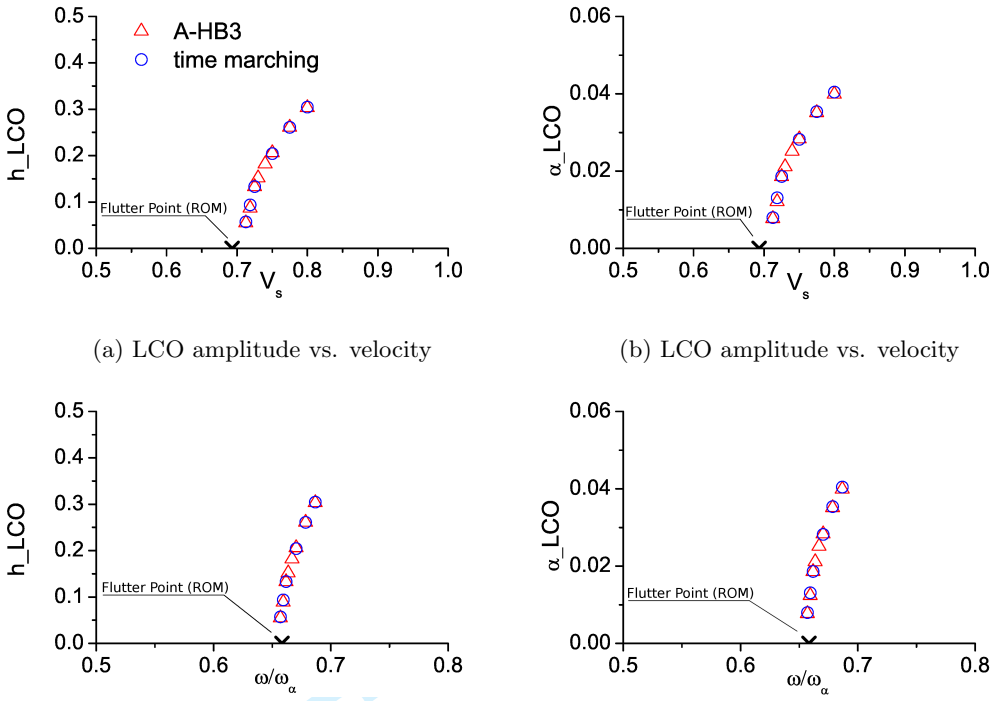

(a) LCO amplitude vs. velocity

(b) LCO amplitude vs. velocity

(c) LCO amplitude vs. frequency ratio

(d) LCO amplitude vs. frequency ratio

Fig. 14 LCO amplitude comparison between A-HB and time marching methods.

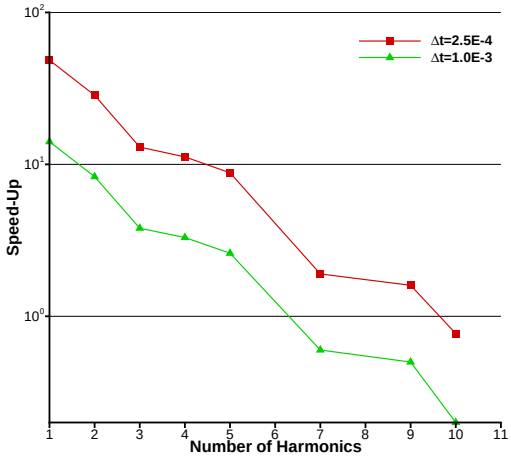

Fig. 15 Relative computational cost with respect to number of harmonics and time-marching method, $V_s = 0.80$

VI. Delta Wing

To further exercise the proposed method, a cropped-delta wing test case derived from reference [13], is explored. The wing plan form is shown in Fig. 16, the wing has a leading edge sweep angle of

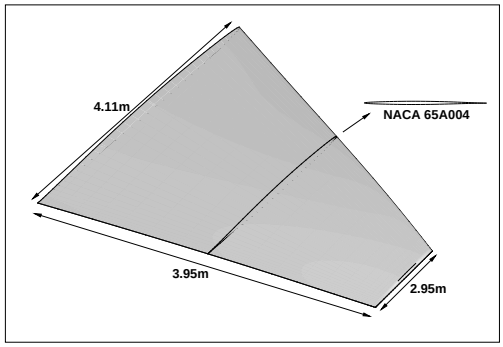

Fig. 16 Delta Wing Geometry and Dimensions

approximately 16°, and a span of just under $4m$. The wing uses a $NACA\ 65A004$ aerofoil. An O-H type grid, shown in Fig. 17-b), was employed for the CFD calculations, a CFD flow-field solution at the nominal conditions of this test case ($M_\infty = 0.91$; $\alpha = 0°$) is shown in Fig. 17-c), where a shock-wave is visible across the span of the wing.

To investigate LCOs, a structural model is coupled with the CFD mesh. The structural model is built in MSC/NASTRAN, using 2D shell elements; the wing material is based on the AGARD 445.6 wing [31], this results in the first four normal modes retained for this analysis to have frequencies in the range of $4Hz - 30Hz$. The mode shapes and natural frequencies are given in Fig. 18. Infinite

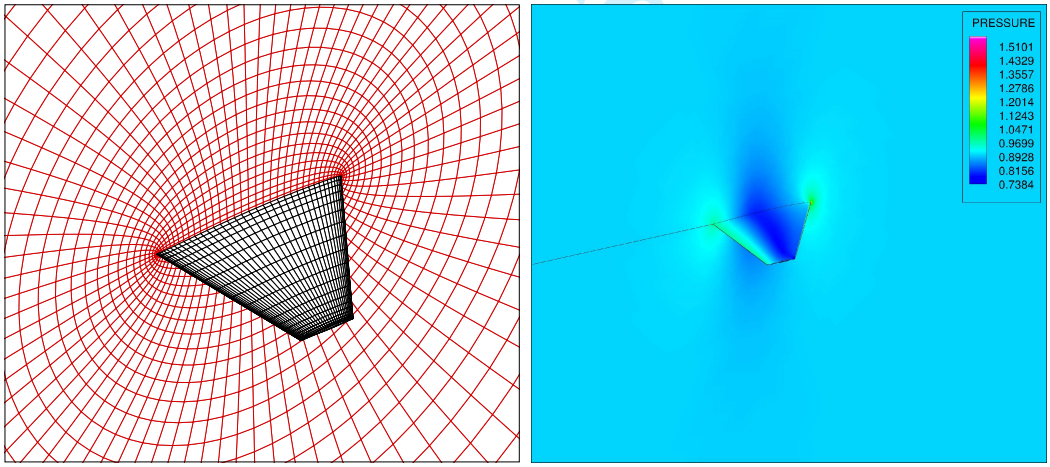

a-) CFD grid - $81 \times 41 \times 41$ b-) Pressure contours, $M_\infty = 0.91$; $\alpha = 0°$

Fig. 17 Delta Wing CFD model - the grid contains $81 \times 41 \times 41$ points, circumferential, radial and span-wise direction, respectively

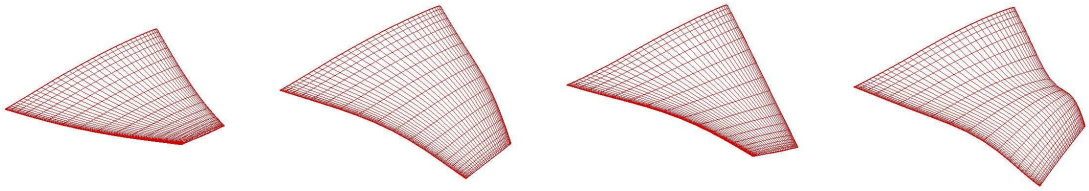

Mode 1 - $3.94Hz$ Mode 2 - $12.88Hz$ Mode 3 - 15.82 Mode 4 - $27.56Hz$

Fig. 18 Structural modes projected onto the CFD grid.

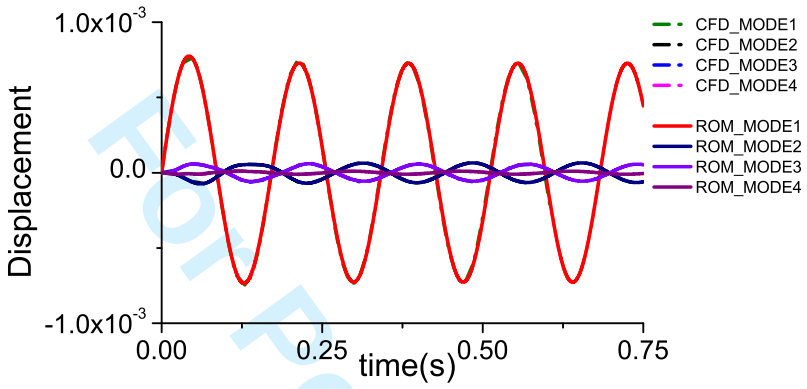

Fig. 19 Delta Wing Flutter response with Volterra Series 808^{th} ROM

Plate Spline (IPS) is used to extrapolate structural modal displacements from the CSD model to the CFD grid, as shown in Fig. 18. The starting point of this LCO investigation is the flutter boundary, even though this is not always necessary, since the proposed HB method should deliver a trivial solution below the flutter boundary. As before, the Volterra series along with the ERA method is employed to construct a linear CFD-ROM, in this case retaining 80-DOF, coupled with the structural model to form the ROM and predict the onset of flutter, as shown in Fig. 19. The dynamic pressure corresponding to the onset of flutter at $M_\infty = 0.91$, $\alpha = 0°$, predicted by the ROM is $q = 0.759 q_{sl}$, where q_{sl} is the dynamic pressure at sea level conditions. The CFD response is included for comparison with the ROM results in Fig. 19, the ROM is able to replicate the CFD accurately at flutter conditions.

The initial disturbances for the LCO prediction, in modal coordinates and for each mode are: $[1, 0.5, 0.1, 0.1]^T$, and the initial reduced frequency is: $\kappa = 0.07$. With the exception of Table 5, all

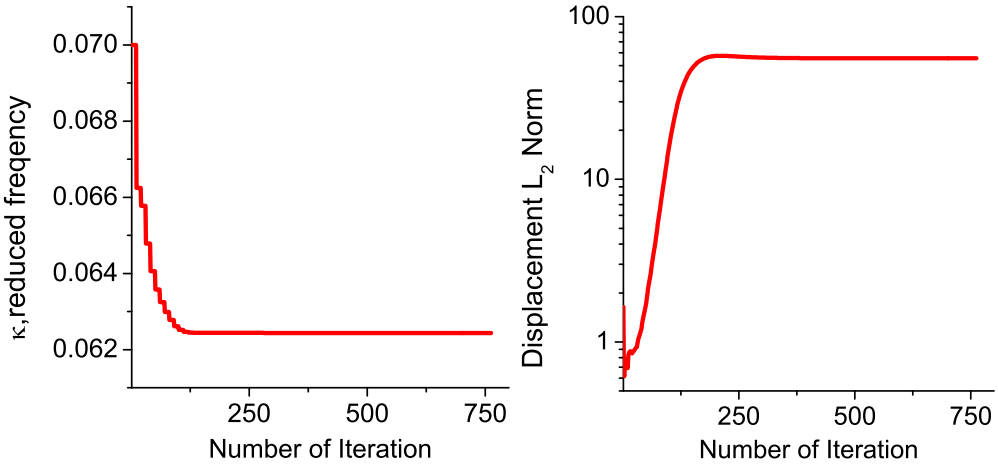

LCO Frequency Convergence LCO Amplitude Convergence

Fig. 20 Delta Wing LCO Response Convergence with A-HB Method

results using the A-HB method presented in this section were obtained retaining one harmonic only. Figure 20 shows the convergence of the A-HB method for the LCO frequency and displacement. The frequency converges within 250 iterations, with the LCO amplitude requiring a further 50 iterations to reach its final value. Two test cases at different free-stream pressures are conducted. The wing undergoes significant oscillations at the wing tip, as indicated by the flow-fields shown in Fig. 21 and the amplitudes in Fig. 22, here η_1 and η_2 correspond to points at the wing tip's leading and trailing edges, respectively. Comparison of LCO responses using the A-HB method against time marching results are also shown in Fig. 22. The flow-fields shown in Fig. 23 compare the time-marching simulation to the A-HB result, the main flow features and patterns are well captured by the A-HB, including the shock towards the trailing edge and the pressure drop at the tip's leading edge. Time-marching results required a time step of 10^{-5} to converge the cycle amplitude, taking 8.5 days on a single core. The current method is able to predict the LCO conditions accurately using one harmonic, reducing the computational time to 8 hours. For this problem, retaining additional harmonics has a small effect on accuracy, as illustrated by Table 5. The scaling of the method for 3D problems is similar to the 2D case investigated, however this test case also exhibits faster convergence rates for the structural residual, which will mitigate the impact of retaining more harmonics when comparing it against the 2D problem investigated.

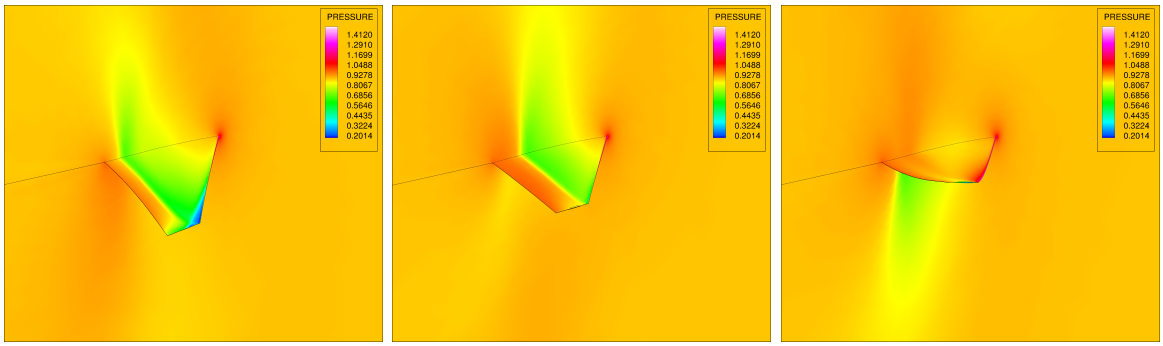

(a) sub-level 1 (b) sub-level 2 (c) sub-level 3

Fig. 21 Delta Wing Pressure Contours snapshots during LCO cycle, $q = 0.900q_{sl}$

N. Harmonics	ω/ω_{LCO}	Speed-up
1 Harmonics	0.9933	25.5
2 Harmonics	1.0001	14.0
3 Harmonics	0.9994	9.7

Table 5 Ratios between frequencies predicted by the A-HB and time-marching methods, $q = 0.850q_{sl}$

VII. Conclusion

This paper presented a new formulation to predict LCOs for aerofoils and fixed wings, using an A-HB methodology. A CFD and CSD system of equations were coupled and solved using a nonlinear HB method. To determine LCO conditions, the coupled system was driven to convergence by updating the aeroelastic system's frequency of motion considering the influence of aerodynamic forces. The new method showed promising results in predicting LCO amplitudes and frequencies for multiple-degree-of-freedom aeroelastic systems, including 2D aerofoils and a delta wing at transonic conditions. Results showed at least an order of magnitude reduction in computational time with respect to conventional time marching methods, without compromising accuracy.

VIII. Acknowledgements

This work was sponsored by the United Kingdom Engineering and Physical Sciences Research Council (grant number EP/K005863/1). The authors gratefully acknowledged this support.

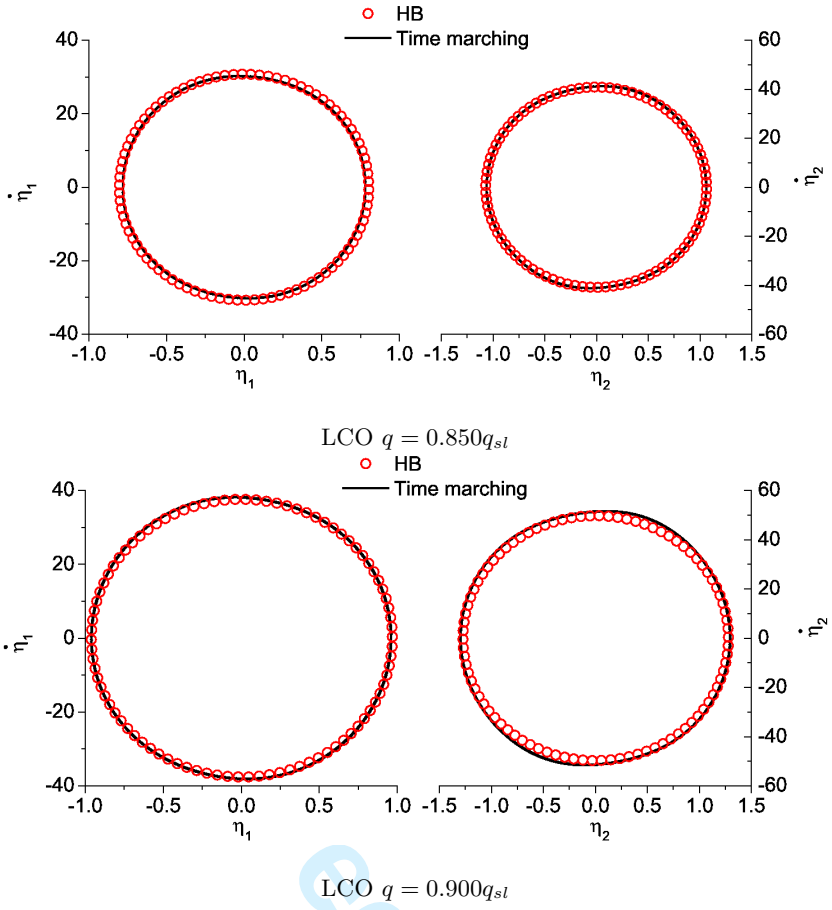

Fig. 22 Delta wing LCO response with A-HB method

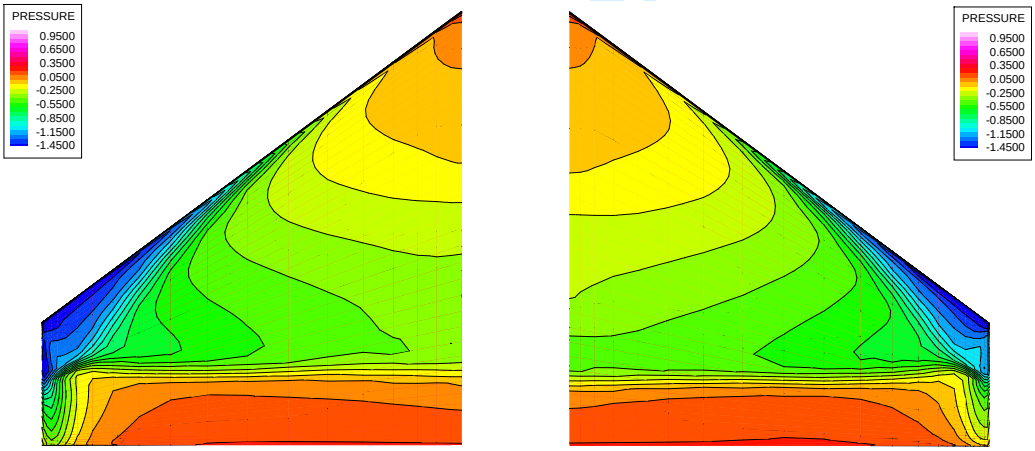

(a) Time-Marching (b) A-HB

Fig. 23 Delta wing upper surface pressure contours snapshot during LCO cycle, $q = 0.900q_{sl}$

REFERENCES

[1] Research Fellow, School of Mechanical and Aerospace Engineering, Queen's University Belfast, Belfast, UK, BT9 5AH, and MAIAA.

[2] Lecturer, School of Mechanical and Aerospace Engineering, Queen's University Belfast, Belfast, UK, BT9 5AH, and MAIAA,.

[3] Noll, T. E., Brown, J. M., Perez-Davis, M. E., Ishmael, S. D., Tiffany, G. C., and Gaier, M., "Investigation of the Helios Prototype Aircraft Mishap," Tech. rep., NASA, 2004.

[4] Bunton, R. and Denegri, C., "Limit Cycle Characteristics of Fighter Aircraft," *Journal of Aircraft*, Vol. 37, No. 5, 2000, pp. 916–918.

[5] Thomas, J., Dowell, E., Hall, K., and Denegri, C., "Modeling limit cycle oscillation behavior of the F-16 fighter using a harmonic balance approach," Tech. rep., AIAA, 2004. Presented at the AIAA/ASME/ASCE/AHS/ASC Structures, Structural Dynamics, and Materials Conference, AIAA Paper 2004-1696.

[6] Marques, S., Badcock, K., Khodaparast, H., and Mottershead, J., "Transonic Aeroelastic Stability Predictions Under the Influence of Structural Variability," *Journal of Aircraft*, Vol. 47, No. 4, 2010, pp. 1229–1239.

[7] Badcock, K. J., Khodaparast, H., Timme, S., and Mottershead, J., "Calculating the Influence of Structural Uncertainty on Aeroelastic Limit Cycle Response," AIAA paper 2011-1741, AIAA, 2011. Presented at the 52nd AIAA/ASME/ASCE/AHS/ASC Structures, Structural Dynamics, and Materials Conference.

[8] Beran, P., Knot, N., Eastep, F., Synder, R., and Zweber, J., "Numerical Analysis of Store-Induced Limit Cycle Oscillarion," *Journal of Aircraft*, Vol. 41, No. 6, 2004, pp. 1315–1326.

[9] Lieu, T., Farhat, C., and Lesoinne, M., "Reduced-order fluid/structure modeling of a complete aircraft configuration," *Computer Methods in Applied Mechanics and Engineering*, Vol. 195, No. 41–43, 2006, pp. 5730–5742,
doi:10.1016/j.cma.2005.08.026. John H. Argyris Memorial Issue. Part {II}.

[10] Silva, W., "Identification of Nonlinear Aeroelastic Systems Based on the Volterra Theory: Progress and Opportunities," *Nonlinear Dynamics*, Vol. 39, No. 1-2, , pp. 25–62,
doi:10.1007/s11071-005-1907-z.

[11] Lucia, D., Beran, P., and Silva, W., "Aeroelastic System Development Using Proper Orthogonal Decomposition and Volterra Theory," *AIAA Journal*, Vol. 42, No. 2, 2005, pp. 509–518.

[12] Munteanu, S., Rajadas, J., Nam, C., and Chattopadhyay, A., "Reduced-order model approach for

aeroelastic analysis involving aerodynamic and structural nonlinearities," *AIAA Journal*, Vol. 43, No. 3, 2005, pp. 560–571.

[13] Yao, W. and Liou, M.-S., "Reduced-Order Modeling for Limit-Cycle Oscillation Using Recurrent Artificial Neural Network," Presented at the 14th AIAA/ISSMO Multidisciplinary Analysis and Optimization Conference.

[14] Badcock, K. and Woodgate, M., "Fast Prediction of Transonic Aeroelastic Stability and Limit Cycles," *AIAA Journal*, Vol. 45, No. 6, 2007, pp. 1370–1381.

[15] Hall Kenneth C., Thomas Jeffrey P., and Clark W. S., "Computation of Unsteady Nonlinear Flows in Cascades Using a Harmonic Balance Technique," *AIAA Journal*, Vol. 40, No. 5, 2002, pp. 879–886, doi:10.2514/2.1754. Doi: 10.2514/2.1754.

[16] Gopinath, A., Beran, P., and Jameson, A., "Comparative Analysis of Computational Methods for Limit-Cycle Oscillations," Presented at 47th AIAA/ASME/ASCE/AHS/ASC Structures, Structural Dynamics, and Materials Conference.

[17] Woodgate, M. and Badcock, K., "Implicit Harmonic Balance Solver for Transonic Flow with Forced Motions," *AIAA Journal*, Vol. 47, No. 4, 2009, pp. 893–901.

[18] Blanc, F., Roux, F.-X., and Jouhaud, J.-C., "Harmonic-Balance-Based Code-Coupling Algorithm for Aeroelastic Systems Subjected to Forced Excitation," *AIAA Journal*, Vol. 48, No. 11, 2010, pp. 2472–2481.

[19] Woodgate, M. and Barakos, G., "Implicit Computational Fluid Dynamics Methods for Fast Analysis of Rotor Flows," *AIAA Journal*, Vol. 50, No. 6, 2012, pp. 1217–1244.

[20] Ekici, K. and Hall, K., "Harmonic Balance Analysis of Limit Cycle Oscillations in Turbomachinery," *AIAA Journal*, Vol. 49, No. 7, 2011, pp. 1478 – 1487.

[21] Sicot Frédéric, Gomar Adrien, Dufour Guillaume, and Dugeai Alain, "Time-Domain Harmonic Balance Method for Turbomachinery Aeroelasticity," *AIAA Journal*, Vol. 52, No. 1, 2014, pp. 62–71, doi:10.2514/1.J051848. Doi: 10.2514/1.J051848.

[22] Roe, P., "Approximate Riemann Solvers, Parameter Vectors, and Difference Schemes," *Journal of Computational Physics*, Vol. 43, No. 2, 1981, pp. 357–372.

[23] van Leer, B., "Towards the ultimate conservative difference scheme. II. Monotonicity and conservation combined in a second-order scheme," *Journal of Computational Physics*, Vol. 14, No. 4, 1974, pp. 361–370, doi:10.1016/0021-9991(74)90019-9.

[24] Thomas, J., Dowell, E., Hall, K., and Denegri, C., "Further investigation of modelling limit cycle

oscillation behaviour of the F-16 fighter using a harmonic balance approach," Tech. rep., AIAA, 2005. Presented at the 46th AIAA/ASME/ASCE/AHS/ASC SDM conference, AIAA Paper 2005-1917.

[25] Thomas, J., Dowell, E., and Hall, K., "Nonlinear Inviscid Aerodynamic Effects on Transonic Divergence, Flutter, and Limit-Cycle Oscillations," *AIAA Journal*, Vol. 40, No. 4, 2002, pp. 638–646.

[26] Davis, S., "NACA 64A010 (NASA Ames Model) Oscillatory Pitching," Report 702, AGARD, 1982.

[27] Batina, J. T., "Unsteady Euler Airfoil Solutions Using Unstructured Dynamic Meshes," *AIAA journal*, Vol. 28, No. 8, 1990, pp. 1381–1388.

[28] Marques, A. N., Simões, C. F. C., and Azevedo, J. L. F., "Unsteady aerodynamic forces for aeroelastic analysis of two-dimensional lifting surfaces," *Journal of the Brazilian Society of Mechanical Sciences and Engineering*, Vol. 28, No. 4, 2006, pp. 474–484.

[29] Da Ronch, A., McCracken, A., Badcock, K., Widhalm, M., and Campobasso, M., "Linear frequency domain and harmonic balance predictions of dynamic derivatives," *Journal of Aircraft*, Vol. 50, No. 3, 2013, pp. 694–707.

[30] Liou, M.-S. and Yao., W., "Flutter Analysis for Turbomachinery Using Volterra Series," Presented at the AASME Turbo Expo Conference, Paper GT2014-25474.

[31] Yates, E., "AGARD standard aeroelastic configurations for dynamic response. Candidate configuration I.-wing 445.6," Nasa-tm-100492, 1987.